Journal of the European Ceramic Society 16 (1996) 545–551

0955-2219(95)00127-1
0955-2219/96/$15.00

Mechanical Property Characterization of 9 Mol% Ce-TZP Ceramic Material — II. Fracture Toughness

G. A. Gogotsi,[a] V. P. Zavada[a] & M. V. Swain[b]

[a]Institute for Problems of Strength, National Academy of Sciences, 252014 Kiev, Ukraine
[b]Department of Mechanical and Mechatronic Engineering, The University of Sydney, NSW 2006, Australia

(Received 5 August 1994; revised version received 28 June 1995; accepted 14 July 1995)

Abstract

Fracture toughness testing of four 9 mol% Ce-TZP materials with differing grain sizes has been conducted. Single edge notched beam tests revealed significant differences in the stable force–displacement response during crack extension between these materials. In all instances there was a marked difference between optical and compliance estimates of crack length. This leads to two estimates of the R*-curve response for all the materials. Acoustic emission and transformation zone size was also monitored during crack extension. The observations are discussed in terms of autocatalysis of the phase transformation in Ce-TZP materials.*

1 Introduction

Fracture toughness estimation of Ce-TZP materials has been conducted by a number of authors.[1–4] In all instances very large transformation zones and high fracture toughness values have been obtained. However, such large and non-uniform zones about the crack tip are different from other phase transforming partially stabilized ceramics (Mg-PSZ or Y-TZP). This observation has led to modelling analysis by Marshall[5] and more recently Stump[6,7] has presented a simulation of this behaviour.

In a previous study of the same Ce-TZP materials, Liu *et al.*[4] showed that the measured fracture toughness depended upon the sample testing geometry and basis of interpretation of the data. The size and shape of the transformation zone depended upon whether tests were conducted on single edge notched beam (SENB) or compact tension (CT) geometries. The fracture toughness and zone size were smaller in the SENB than the CT test pieces. Also the form of the *R*-curve was very different, depending upon whether linear elastic fracture mechanics (LEFM) or a *J*-integral approach was adopted for interpretation of the data. There is some question as to whether the *J*-integral is a valid approach because of the nature of the 'plasticity' about the crack tip and, as will be discussed here, the estimation of crack length.

This paper presents SENB observations of crack extension in relatively small samples. The crack extension is followed by monitoring changes in compliance, optical crack length and acoustic emission (AE). From such data the *R*-curves are calculated and related to AE events and transformation zone area.

2 Experimental Procedures

The materials evaluated have been described in Part I of this study.[8] Fracture toughness tests were performed in a three-point flexure rig with a 20 mm span between supports. Specimens were of dimensions 4·8 × 2·8 × 25 mm with an initial notch of 2·4 mm. To facilitate optical observations of nucleation and propagation of crack extension and transformation zone size, one of the specimen lateral sides was polished. AE signals and precision deflection were determined in the manner described in Part I.[8]

3 Observations and Discussion

3.1 Force–displacement behaviour

Force–displacement observations during crack extension of the four Ce-TZP samples are shown in Figs 1–4. In all instances the crack extension behaviour was very stable. The residual crack opening displacement increased with grain size from Ce-TZP-I to Ce-TZP-IV. Also the onset of crack growth, particularly in the case of Ce-TZP-III an Ce-TZP-IV did not occur until significant offset (marked on the figures) of the force–displacement curve. The numbers within the loops relate to the load–unloading cycles.

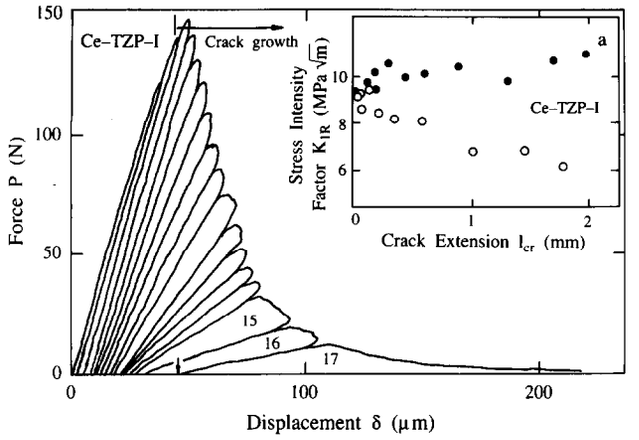

Fig. 1. Force–displacement data during crack extension of Ce-TZP-I. The arrows at the bottom of the figure are where the photographs of the crack tip were taken. The number within the loop is the fracture cycle. Inset shows the computed stress intensity factor versus crack extension l_{cr}. (●), Optically measured crack length; (○), compliance estimates of crack length.

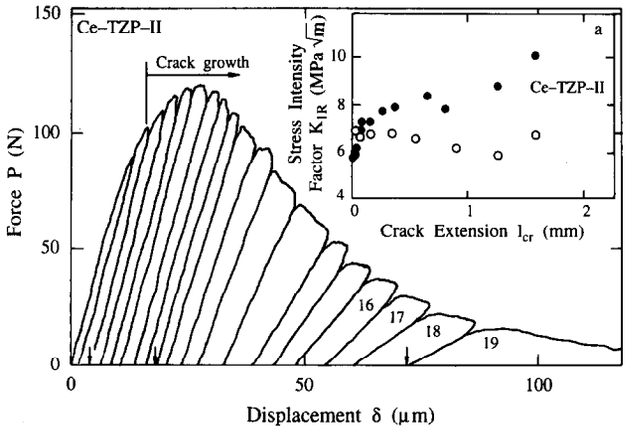

Fig. 2. Force–displacement data for crack extension in Ce-TZP-II. Inset shows computed stress intensity factor versus crack extension for optical and compliance estimates of crack length.

3.2 Fracture toughness: *R*-curves

Two approaches were used to estimate the fracture toughness, the optical measurement of the crack length and that from the compliance of the load–unloading curves in Figs 1–4. The two calculations of critical stress intensity factor versus crack length are shown in the insets to Figs 1–4. In both instances the stress intensity factor was calculated from the standard relationship:[9]

$$K = Y(a/W)\sigma \sqrt{a} \qquad (1)$$

where $Y(a/W)$ is the usual modifying factor, σ is the nominal flexure stress from peak load in the absence of a crack, a is the crack length and W the specimen width.

The *R*-curves determined from the compliance and optical observations show different trends. From the optical measurements the *R*-curve appears to increase with crack extension, whereas from the compliance measurements the toughness appears to decrease with crack extension. This

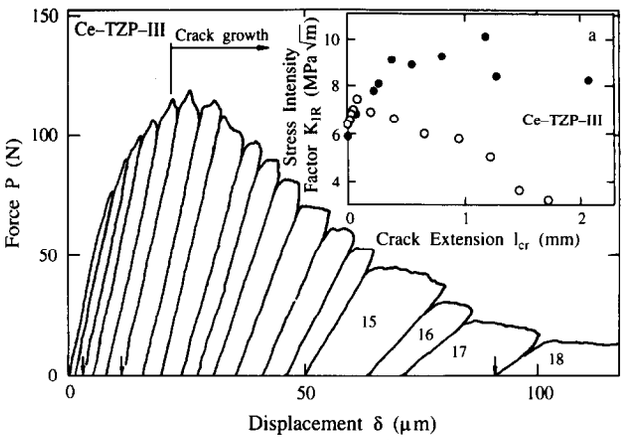

Fig. 3. Force–displacement data for crack extension in Ce-TZP-III. Inset shows computed stress intensity factor versus crack extension for optical and compliance estimates of crack length.

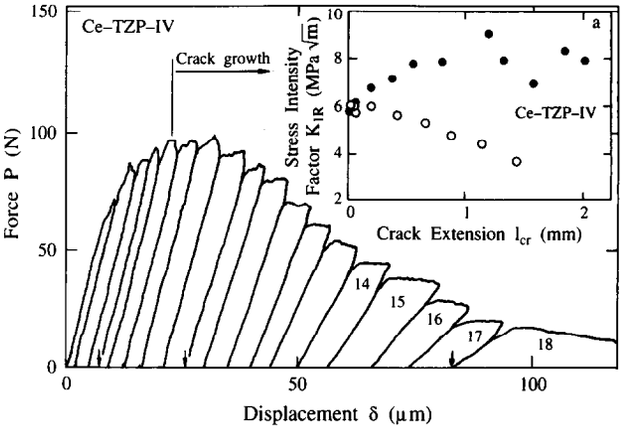

Fig. 4. Force–displacement data for crack extension in Ce-TZP-IV. Inset shows computed stress intensity factor versus crack extension for optical and compliance estimates of crack length.

Table 1. Grain size and work of fracture for Ce-TZP ceramics

Material	*Grain size (μm)*	$\gamma(J\,m^{-2})$	$K_c = \sqrt{2\gamma E}\ (MPa\ m^{1/2})$
Ce-TZP-I	1·14	308	10·4
Ce-TZP-II	1·62	454	12·6
Ce-TZP-III	2·22	494	13·1
Ce-TZP-IV	3·0	452	12·6

arises from the significant differences in the estimated crack lengths from the two approaches used. From the peak load values and calculated *R*-curves, Ce-TZP-I is tougher than the remaining samples. However, if one compares the work of fracture calculated from the area under the entire force displacement curve a different conclusion is reached; namely that Ce-TZP-III has the highest toughness, as listed in Table 1.

3.3 Compliance observations

The compliance values for all the load cycles were measured directly from the slopes of the loading-unloading cycles in Figs 1–4. The crack length was calculated from the specimen compliance using the relationship:[10]

$$\frac{C^c}{C_o} = 1 + 4{\cdot}5 \int_o^{\alpha} [Y(\alpha)]^2 \, \alpha \, d\alpha \qquad (2)$$

where C_o is the specimen compliance without a notch, C^c is the compliance measured experimentally, Y is the modifying parameter after Strawley[11] and $\alpha = a/W$.

The difference between optical and compliance estimates of the crack length are shown in Fig. 5 for all the Ce-TZP materials. In all instances the compliance estimates of crack length a^c are much less than the optically measured a^o values. More critical appreciation of the influences of the individual microstructures on this difference may be seen by comparing the ratio of the optical to the measured compliance (C^o/C^c) versus optically measured crack length, as shown in Fig. 6. A simple linear relationship was found to exist between these parameters which could be expressed by:

$$\frac{C^o}{C^c} = A + k_3 \, a^o \qquad (3)$$

The basis for these differences in compliance being caused by measurement errors is excluded, as

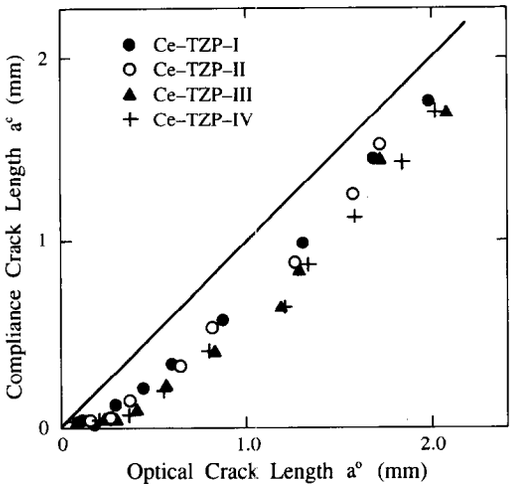

Fig. 5. Comparison between optical a^o and compliance a^c estimates of crack length for Ce-TZP materials.

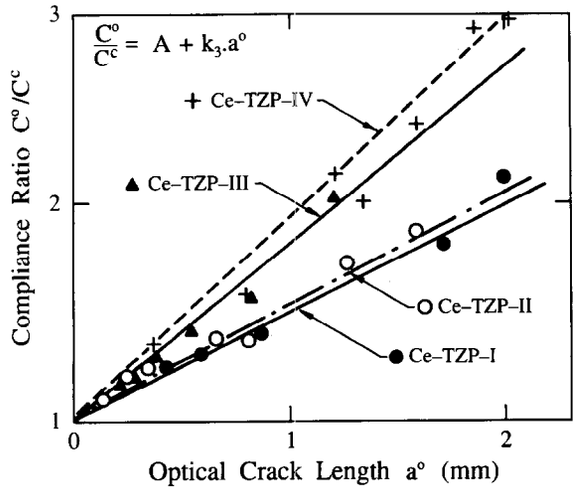

Fig. 6. Plot of ratio of optical and measured compliance (C^o/C^c) versus optically measured crack length a^o.

excellent correlation between the two approaches has been previously reported by Gogotsi *et al.*[12] for other non-transforming ceramics including glass and polycrystalline alumina. It is also argued that optical measurement errors would tend to underestimate crack length and further increase the discrepancy found in Fig. 5 because of the very narrow crack opening displacement near the crack tip. Errors in the determination of the slope of the load-displacement curves of Figs 1–4 and thereby the estimated compliance do not exceed 5%, whereas the discrepancy between the optical and determined compliance reaches more than 200%.

The slope of the ratio of C^o/C^c shows a clear increase with Ce-TZP materials I to IV, which corresponds to the increase in grain size.[8] The discrepancy between a^c and a^o, C^c and C^o leads to uncertainty in the estimation of the J-integral value for toughness. This arises because the J-integral is calculated with the aid of both load–displacement curves, as well as the actual crack length. In the current situation the contradictory features of both these measurements are likely to compound errors in its calculation.

3.4 Transformation zones

Optical observations of the transformation zone about the notch and crack tip were made at the positions marked by arrows in Figs 1–4. These micrographs are shown in Figs 7–10. No pronounced transformation zone was observed during the fracture toughness testing of the Ce-TZP-I material for different crack lengths (Fig. 7). However the force displacement observations (Fig 1) and the optical micrographs (Fig 7) show significant residual crack opening displacement. Whereas, for the remaining materials, the transformation zones were clearly visible in a manner that enabled both the complex shape of the zone and the crack length to be appreciated. For Ce-TZP-II to Ce-TZP-IV the cycle by cycle observations revealed that the zones did not grow in a continuous manner but rather in jump-like needle-shaped zones of different widths and lengths emanating from the notch region. There is a trend of increasing length and width of such zones for materials II to IV. As the load increases the number of bands increases and they coalesce forming a continuous zone at the notch tip which then re-extends as several separate needle-like zones. A crack usually nucleates within the continuous zone, and as the crack grows this continuous zone also advances ahead of the crack tip.

From the observations in Figs 7–10 the area of transformation about the crack tip as a function

Fig. 7. Optical micrograph of the notch and crack extending from the notch in Ce-TZP-I. The photograph (at × 70) was taken at the position arrowed in Fig 1.

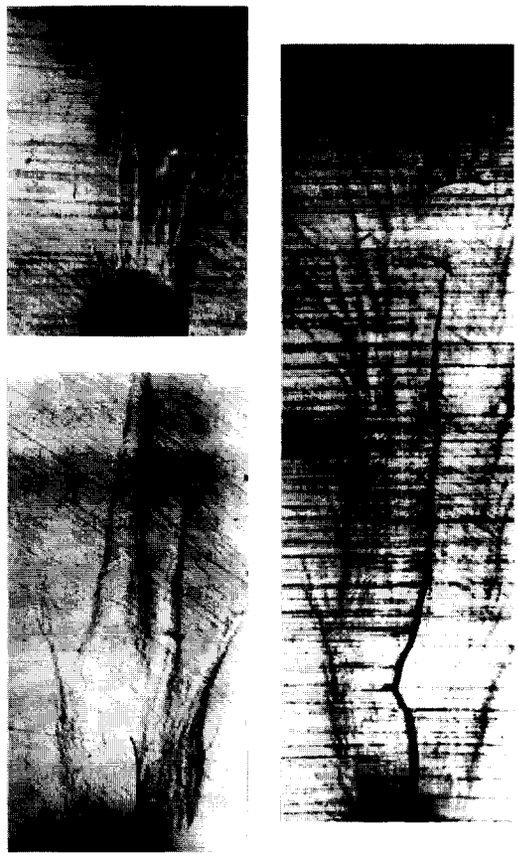

Fig. 8. Micrographs of the crack and associated transformation zone during crack extension in Ce-TZP-II. The photograph (at × 70) was taken at the positions arrowed in Fig. 2.

of crack extension may be estimated. Such measurements are shown in Fig. 11. A linear relationship may be readily fitted to the data relating the transformation zone area S to the crack length, namely:

$$S = S_o + k_4 a^o \quad (4)$$

In Fig. 11 S_o, the intercept, provides an estimate of the precrack nucleation size of the transformation zone about the initiating notch. Then, as shown schematically in Fig. 12, this zone extends ahead of the crack during propagation. Thus it is not surprising that a near one-to-one correlation exists between the slope of the data k_4 and the width of the zone W.

3.5 Acoustic emission

Considerable differences between the AE activity of the different materials were observed. The Ce-TZP-I material did not emit detectable events above the background noise.

The AE events were detected only when a pronounced t → m transformation zone is formed and there appears to be no correlation between the number of AE events (N_Σ) and the transformed area (Fig. 13). The probable reason for this behaviour is that AE activity is largely determined not by the size of the transformation zone area but the jump-like manner in which it is formed and the number of such occurrences. As shown in Part I of this study,[8] the number of AE counts was correlated with the number of bands rather than their width.

Another feature from the results in Fig. 13 is that the commencement of AE activity did not coincide with crack nucleation and growth. The absence of AE events in the Ce-TZP-I material, despite their occurrence during the beam flexure testing, suggests that crack growth is accompanied by much lower intensity activity than the burst-like t → m transformations. The results for the Ce-TZP-I would indicate that without burst activity AE events do not occur. The absence of AE activity and any discernable transformation zone about the crack tip, despite the significant residual crack opening displacement, is consistent with the observations made in Part I of this study.[8] In the previous paper the residual flexural displacement upon unloading did not correlate with the number of transformation bands and in fact the initial permanent set occurred in the absence of any bands or AE activity. It was suggested that this may be due to ferroelastic grain reorientation occurring upon the stress level exceeding a critical value and then, at a higher stress level, transformation and

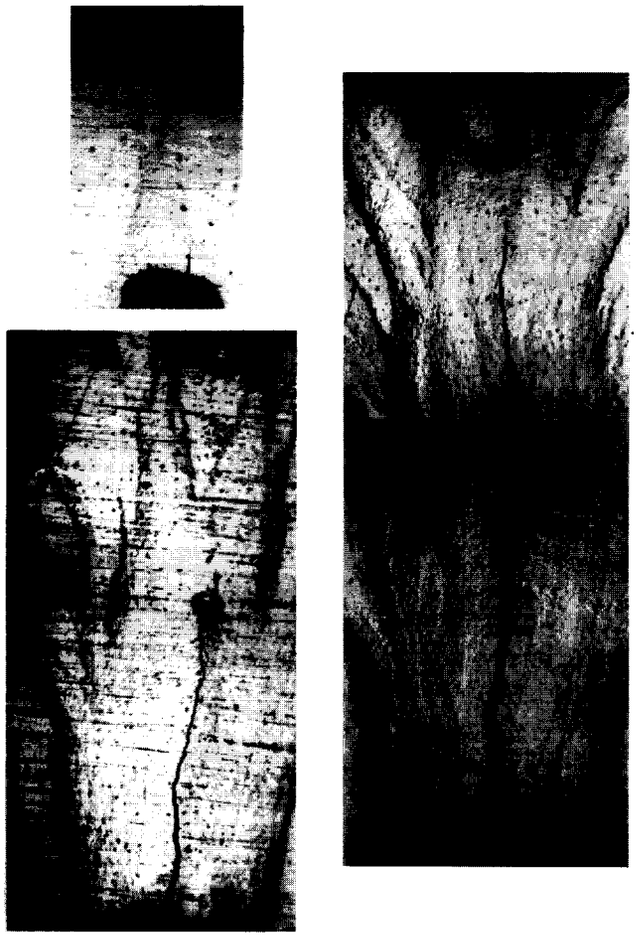

Fig. 9. Micrographs of the crack and associated transformation zone during crack extension in Ce-TZP-III. The photograph (at × 70) was taken at the positions arrowed in Fig 3.

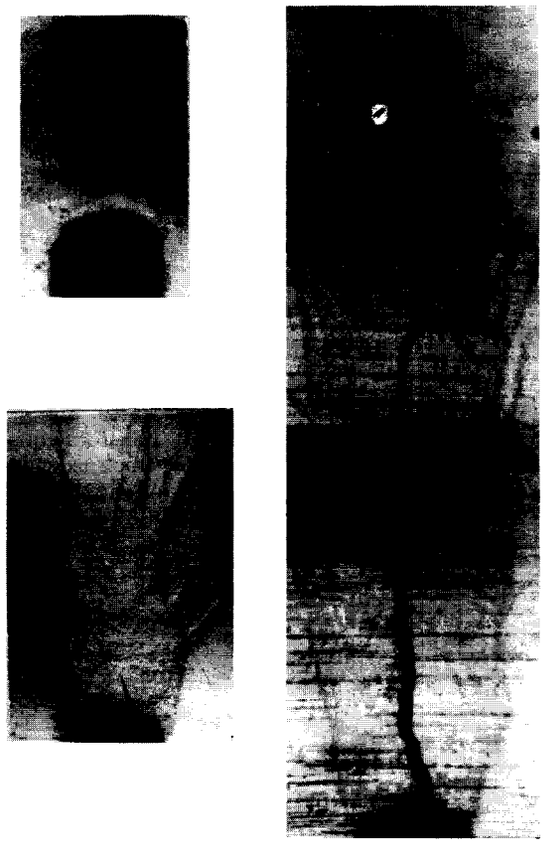

Fig. 10. Micrographs of the crack and associated transformation zone during crack extension in Ce-TZP-IV. The photograph (at × 70) was taken at the positions arrowed in Fig. 4.

the occurrence of bands on the tensile surface. Matsumoto and Virkar[13] have previously suggested such behaviour in a Ce-TZP material on the basis of X-ray analysis of ground surfaces.

Continuous AE monitoring of complete load–unload crack extension cycles revealed that events also occurred during unloading. A typical example of such behaviour is shown in Fig. 14. In this instance the unloading curve is non-linear and does not coincide with the subsequent reloading line. Such observations suggest that ligaments and bridges behind the crack tip may fracture during the unloading cycle, thereby changing the specimen compliance and also contributing AE activity. Other evidence in support of ligament formation was the regularly observed feature of the main crack arresting and a new crack either initiating from the notch or adjacent to the main crack.

3.6 Interpretation

In recent papers Stump[6,7] has addressed the issue of autocatalysis and the role of shear stresses on the transformation zone formation in this class of materials. In particular, in a simulation study where he systematically varied the shear and dilational strains associated with transforming particles, the shape of the transformation about the crack tip changed from a near cardiod form for purely dilational strain to needle-like for primarily shear strain dominated transformation.

However, in order to make use of the concepts and simulation proposed by Stump, definitions and estimates of some of the parameters he used need to be defined, where possible, for the present materials. The characteristic length dimension, comparable to the plastic zone dimension for metallic materials, is given by:[6,7]

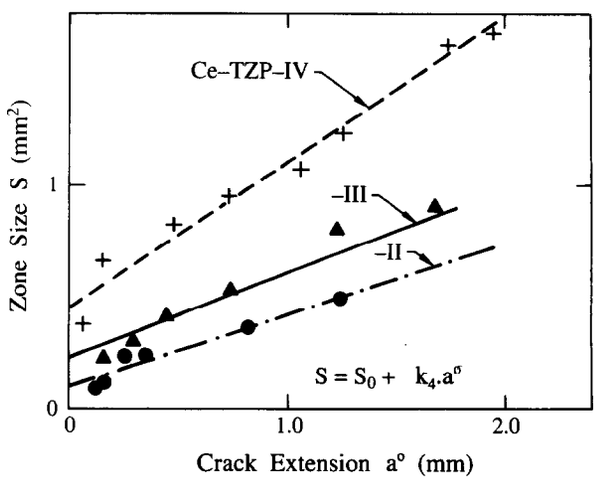

Fig. 11. Plot of the area of the transformation zone size as a function of crack length for Ce-TZP-II to Ce-TZP-IV.

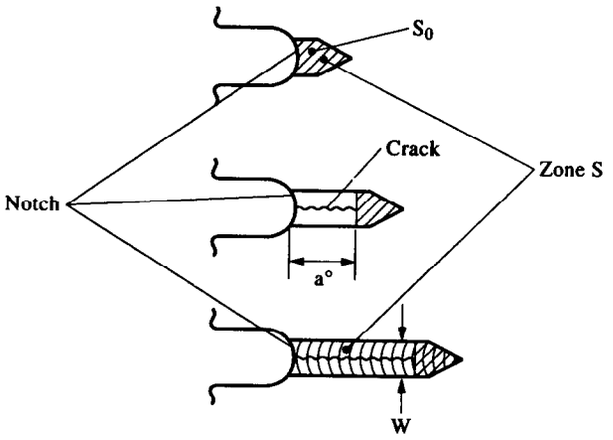

Fig. 12. Schematic illustration of the transformation zone about the notch and crack tip as the crack extends. Also marked are the dimensions of the transformation zone width W, crack length a^o and area of transformation S.

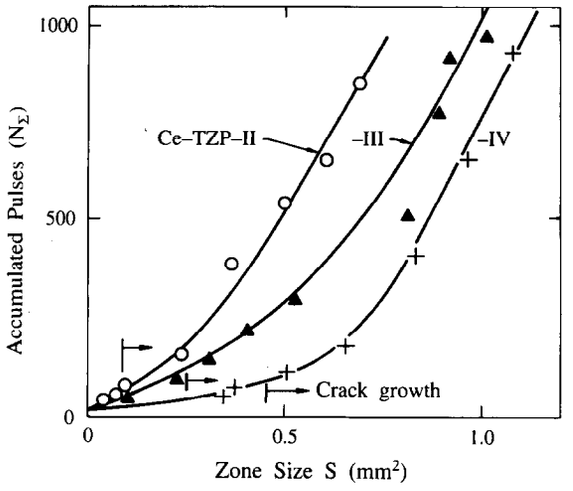

Fig. 13. Interrelation between accumulated acoustic emission events N_Σ and transformation zone area S. Arrows mark the onset where crack growth initiates.

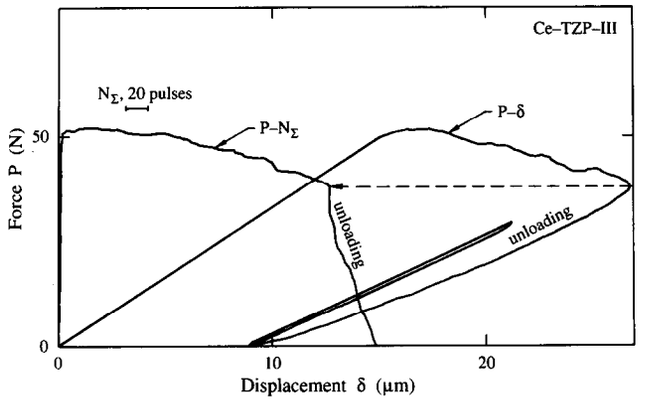

Fig. 14. Acoustic emission monitored during complete loading and unloading cycle for Ce-TZP-III. Note the acoustic emission events during unloading.

$$L_o = \frac{2}{9\pi}\left[\frac{K_m(1+\upsilon)}{\sigma^c{}_m}\right]^2 \text{ or } L = \frac{1}{8\pi}\left(\frac{K_m}{\sigma_c}\right)^2 \quad (5)$$

where K_m is the crack tip stress intensity factor for fracture (K_m ~3 MPa $m^{1/2}$), $\sigma^c{}_m$ is the critical mean stress to trigger the transformation and σ_c is the critical tensile stress for the deviation from linearity during tensile or flexure testing. The transformation-toughening parameter, or measure of the magnitude of the toughening increment is given by:[6,7]

$$\omega = \frac{Ec_t\theta^T}{\sigma^c{}_m}\left(\frac{1+\upsilon}{1-\upsilon}\right) \quad (6)$$

where c_t is the volume fraction of transformed tetragonal phase and θ^T the dilational strain associated with transformation. Stump introduces two more parameters that quantify the dilational strain β and shear strain ρ associated with the transformation of a particle; namely

$$\beta = \frac{E\theta_T}{\sigma_c(1-\upsilon)}, \quad \rho = \frac{E\gamma_T}{\sigma_c(1-\upsilon^2)} \quad (7)$$

where γ_T is the transformation shear strain. Taking typical values for the current materials, namely E from Ref. 8, $\upsilon = 0{\cdot}25$, $K_m = 3$ MPa $m^{1/2}$, $\theta_T = 0{\cdot}04$, $\gamma_T = 0{\cdot}05$ and values for σ_c again taken from the previous paper[8] (see Fig. 1), leads to the estimates for β, L and ρ given in Table 2.

Table 2. Estimates of transformation parameters for Ce-TZP materials

Material	σ_c*(MPa)*[8]	β	*L(μm)*	ρ	*E(GPa)*[8]
Ce-TZP-I	216	43·2	7·6	43·8	175
Ce-TZP-II	168	56·8	12·8	57·6	179
Ce-TZP-III	156	61·9	14·8	62·7	181
Ce-TZP-IV	138	68·0	18·9	68·9	176

The calculated values of β and ρ appear to be very large because of the low values of σ_c measured for the present Ce-TZP materials. In fact these values are all beyond the range that Stump[6] simulated. One possible explanation as to why these estimates are excessive is that no account of the extent of the phase transformation within the crack initiated transformation zone is allowed for in the expressions [eqn (7)].

Thus, possibly a better estimate for β and ρ would be to include a factor c_t in eqn (7) which is the volume fraction of phase transformation within the zone, typically ~50% or less, although not measured for the present materials. Such an approach would approximately halve the values of β and ρ estimated.

The increasing values of β and ρ for materials II to IV and the nature of the observed transformation zone shapes would appear to confirm the simulations by Stump,[6] provided that for the Ce-TZP materials the ratio of shear to mean tensile stress criteria for transformation was <1. However this approach does not account for the apparent absence of any transformation about the crack

tip for the Ce-TZP-I material. Liu *et al.*[4] also did not observe a transformation zone for the same material when tested in either SENB or CT geometries. Liu *et al.*[4] did, however, observe that the shape and size of the zone from the other materials was much greater for CT geometries, presumably because of the lower likelihood of initiating a transformation zone 'hinge' between the crack tip and the rear surface with SENB geometries.

4 Summary and Conclusions

The present studies have shown that 9 mol% Ce-TZP ceramics exhibit very extensive transformation zones about loaded notches and crack tips. The size of these zones increases with grain size and the shape of the zones are comparable to the simulations of Stump.[6,7]

The measured fracture toughness versus crack extension showed opposite trends dependent upon whether the optical or measured compliance value for crack length was used. In all instances the measured compliance was greater than that calculated from optical measurements. A linearly increasing ratio of these two estimates with crack extension was observed, the slope of which increased with grain size and transformation zone size of the Ce-TZP. No evidence of a transformation zone about the crack tip in the finer grained Ce-TZP-I was seen. It is suggested that the high toughness of this material may be due to ferroelastic grain reorientation occurring about the crack tip.

Transformation zone size area increased linearly with crack extension with an intercept at zero crack growth, indicating that transformation has occurred about the notch region prior to crack initiation. No correlation between AE events and area of phase transformation was found. More events per unit of transformation area were found for the finer grained Ce-TZP-II than for the coarser grained Ce-TZP-IV material. AE events were also detected during unloading which may have occurred because of further crack extension or phase transformation.

Acknowledgements

The authors wish to thank Drs T.-S. Liu and G. Grathwohl for provision of materials and comments on the text.

References

1. Rose, L. R. F. & Swain, M. V., Transformation zone shape in ceria-partially stabilised zirconia. *Acta Metall.*, **36** (1988) 955–62.
2. Grathwohl, G. & Liu, T., Crack resistance and fatigue of transforming ceramics: II. CeO_2 — stabilised tetragonal ZrO_2. *J. Am. Ceram. Soc.*, **74** (1991) 3028–34.
3. Yu, C.-S. & Shetty, D. K., Transformation zone shape, size, and crack growth resistance (*R*-curve) behaviour of ceria-partially-stabilised zirconia polycrystals. *J. Am. Ceram. Soc.*, **72** (1989), 921–8.
4. Liu, T., Mai, Y.-W., Swain, M. V. & Grathwohl, G., Transformation and *R*-curve behaviour of 9 Ce-TZP ceramics: Part 1, grain size and specimen geometry effects. *J. Am. Ceram. Soc.*, in press.
5. Marshall, D. B., Crack tip shielding in ceria partially stabilised zirconia. *J. Am. Ceram. Soc.*, **73** (1990) 3119–21.
6. Stump, D. M., The role of shear stresses and shear strains in transformation toughening. *Phil. Mag. A*, **64** (1991) 879–902.
7. Stump, D. M. & La Violette, R. A., Effects of shear stresses on crack growth microstructures in transformation toughened ceramics. *Phil. Mag. A*, **68** (1993) 35–47.
8. Gogotsi, G. A., Zavada, V. P. & Swain, M. V., Mechanical property characterisation of a 9 mol% Ce-TZP ceramic material: I. Flexural response. *J. Europ. Ceram Soc.*, **15** (1995) 1185–92.
9. Atkins, A. G. & Mai, Y.-W., *Elastic and Plastic Fracture.* Ellis Horwood, Chichester, 1985.
10. Kleinlein, F. W. & Hubner, H., The evaluation of crack resistance and crack velocity from controlled fracture experiments of ceramic bend specimens. *Fracture*, **4** (1977) 838–41.
11. Strawley, J. E., Wide range stress intensity factor expression for ASTM E-339 standards fracture toughness specimens. *Int. J. Fracture*, **12** (1976) 475–6.
12. Gogotsi, G. A., Zavanda, V. P. & Fesenko, A. I., Method and results R-curve determination in ceramics. Zavodsaya Laboratoriya (Ind. Lab.), **58** (1992) 40–3 (in Russian).
13. Virkar, A. V. & Matsumoto, R. L. K., Ferro-elastic domain switching as a toughening mechanism in tetragonal zirconia. *J. Am Ceram. Soc.*, **69** (1986) C224–6.